JOURNAL OF MATERIALS SCIENCE 26 (1991) 2507–2513

Crystal twinning in simultaneous biaxial stretching of gelation-crystallized ultra-high molecular weight polyethylene

MYUNG H. CHO, SADAO HIBI*, THEIN KYU‡
Institute of Polymer Engineering, University of Akron, Akron, OH 44325, USA

Structure and orientation development in simultaneous biaxial stretching of gelation-crystallized ultra-high molecular weight polyethylene (UHMWPE) was examined by means of X-ray pole figures. The dry gel film exhibits a stacked lamellar structure similar to single-crystal mats with preferential crystal *c*-axis orientation normal to the film surface. The biaxially stretched gelation-crystallized films reveal a complex crystal orientation of (1 1 0), (2 0 0) and (0 2 0) planes. The detailed analysis of these pole figures manifests the occurrence of crystal twinning in addition to the orientation of crystallites. Crystal transformation of orthorhombic to monoclinic structure was not observed during biaxial stretching. The orientation distribution functions of crystallites were calculated assuming affine deformation. The orthogonality of crystal $\langle 1\,1\,0\rangle - c$ axes and crystal $a-c$ axes was further assumed to be conserved during the crystal twinning and biaxial orientation, respectively. Model simulation with contributions of 30% crystal twinning and 70% crystal orientation yields the best fit with the X-ray pole figures of biaxially stretched UHMWPE films. The affine model appears to be valid up to a biaxial draw ratio of 1.8 × 1.8, after which the results deviate from ideality with increasing draw ratio.

1. Introduction

The understanding of deformation processes in fabricated polymer parts has been of central importance because of the intimate relation of polymer structure and properties. It is therefore natural to witness numerous studies on the characterization of molecular orientation in relation to mechanical performance of the materials. In highly crystalline polymers, crystal orientation is often accompanied by crystal transformation and/or twinning during cold-rolling or drawing. Frank *et al.* [1] investigated deformation mechanisms in cold-rolled polyethylene and the results were interpreted in terms of crystal plasticity. $(1\,0\,0)[0\,1\,0]$ slip and $(3\,1\,0)(3\,\bar{1}\,0)$ and/or $(1\,1\,0)(1\,\bar{1}\,0)$ twinning were found to be dominant, whereas $(1\,1\,0)[1\,\bar{1}\,0]$ slip appeared to be a less easy mode of deformation compared with the above mechanisms. Under certain conditions, a second crystalline phase occurred associated with phase transformation.

A more detailed study on the orientational processes occurring during the drawing of polyethylene single crystals was undertaken by Geil and co-workers [2–5] with emphasis on the twinning of the orthorhombic unit cell and a phase transformation to a monoclinic unit cell. Various types of deformation, involving different combinations of twinning and phase transformations, were subsequently proposed. The authors pointed out that when the draw direction is near the *b* axis or nearly parallel to the $\langle 1\,1\,0\rangle$ or at an angle between the *b* axis and $\langle 1\,1\,0\rangle$, the phase transformation predominantly occurred in a manner dependent upon the relative direction of crystal axes and the drawing. When the drawing is near the *a* axis, the twinning of $\{1\,1\,0\}$ orthorhombic crystals is the dominant mechanism. The present gelation-crystallized ultra-high molecular weight polyethylene (UHMWPE) has a single-crystal mat structure with preferential *c*-axis orientation in the film normal direction. The *b* axis appears to be random in the film plane. We now explore how crystal twinning and phase transformation would occur during simultaneous biaxial stretching of these gelation-crystallized UHMWPE films.

In a previous paper [6], we reported mainly on the orientation development during simultaneous biaxial stretching. The biaxial orientation was evaluated using wide-angle X-ray (WAXD) pole figures and infrared dichroic methods. The tensile strength and modulus of biaxial films were approximately the same in all directions, indicating uniform mechanical performance. Moreover, these values were comparable to those of uniaxial films of comparable draw ratios. Our analysis on crystal orientation was rather qualitative in a strict sense. In this paper, we examine the pole figures quantitatively in terms of the orientation distribution function. We realize that some of the intensity

---

* On leave from Department of Materials Science and Engineering, Nagoya Institute of Technology, Nagoya, Japan.
‡ To whom correspondence should be addressed.

0022–2461/91 $03.00 + .12

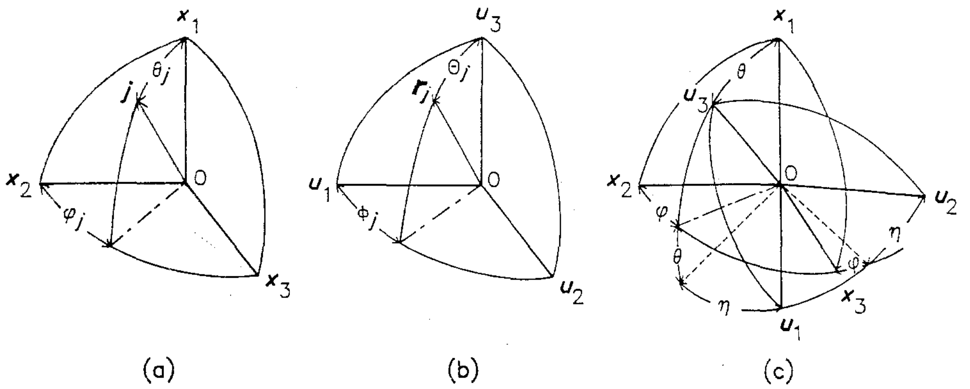

Figure 1 (a) The Cartesian coordinate $0\text{–}x_1x_2x_3$, (b) the principal axes $0\text{–}u_1u_2u_3$ of the crystal and (c) Eulerian angles φ, θ and η specifying the relation between the above two coordinates.

maxima in the pole figures cannot be interpreted solely by the crystal orientation. An additional process such as crystal twinning must be taken into account for explaining the complete pole figures [7, 8].

2. Theoretical background

A transformation matrix a_{im}, which characterizes the orientation of a Cartesian coordinate $0\text{–}u_1u_2u_3$ of a structural unit with respect to a reference Cartesian coordinate $0\text{–}x_1x_2x_3$ in the bulk specimen (laboratory coordinate), may be described in terms of three Euler angles θ, φ, and η:

$$a_{im} = \begin{bmatrix} \cos\varphi\cos\theta\cos\eta & -\cos\varphi\cos\theta\sin\eta & \sin\theta\cos\varphi \\ -\sin\varphi\sin\eta, & -\sin\varphi\cos\eta, & \\ \sin\varphi\cos\theta\cos\eta & -\sin\varphi\cos\theta\sin\eta & \sin\theta\sin\varphi \\ +\cos\varphi\sin\eta, & +\cos\varphi\cos\eta, & \\ -\sin\theta\cos\eta, & \sin\theta\sin\eta, & \cos\theta \end{bmatrix} \tag{1}$$

where a_{im} can be interpreted as the direction cosine of the axis u_m of the structural unit with respect to the axis x_i of the bulk specimen (Fig. 1). For simplicity, Equation 1 may be rewritten as

$$\begin{bmatrix} l_1 \\ l_2 \\ l_3 \end{bmatrix} = a_{im}\begin{bmatrix} l_a \\ l_b \\ l_c \end{bmatrix} = \begin{bmatrix} a_{21}, & a_{22}, & a_{23} \\ a_{31}, & a_{32}, & a_{33} \\ a_{11}, & a_{12}, & a_{13} \end{bmatrix}\begin{bmatrix} l_a \\ l_b \\ l_c \end{bmatrix} \tag{2}$$

where l_i and l_m are the unit vectors of the $0\text{–}x_1x_2x_3$ and $0\text{–}u_1u_2u_3$ coordinates, respectively. The subscripts *a*, *b* and *c* stand for crystal *a*, *b* and *c* axes. The orthogonality condition of the components of directional cosine requires that

$$a_{1i}^2 + a_{2i}^2 + a_{3i}^2 = 1 \qquad i = 1, 2, 3 \tag{3}$$

When an arbitrary vector r_c along the u_3 axis is subject to deformation, it changes to r_c' such that

$$r_c\begin{bmatrix} \lambda_{2c}a_{23} \\ \lambda_{3c}a_{33} \\ \lambda_{1c}a_{13} \end{bmatrix} = r_c'\begin{bmatrix} a_{23}' \\ a_{33}' \\ a_{13}' \end{bmatrix} \tag{4}$$

where λ_{ic} represents the draw ratio in each direction.

Rewriting Equation 4, one obtains

$$r_c'^2 = r_c^2/A_{3c} \tag{5}$$

where

$$A_{3c} = \left(\frac{a_{23}'}{\lambda_{2c}a_{23}}\right)^2 = \left(\frac{a_{33}'}{\lambda_{3c}a_{33}}\right)^2 = \left(\frac{a_{13}'}{\lambda_{1c}a_{13}}\right)^2 \tag{6}$$

Applying Equation 3 to Equation 6 leads to

$$A_{3c} = \left(\frac{a_{23}'}{\lambda_{2c}}\right)^2 + \left(\frac{a_{33}'}{\lambda_{3c}}\right)^2 + \left(\frac{a_{13}'}{\lambda_{1c}}\right)^2 \tag{7}$$

Similarly, one can derive the following expression along the u_1 axis:

$$r_a\begin{bmatrix} \lambda_{2a}a_{21} \\ \lambda_{3a}a_{31} \\ \lambda_{1a}a_{11} \end{bmatrix} = r_a'\begin{bmatrix} a_{21}' \\ a_{31}' \\ a_{11}' \end{bmatrix} \tag{8}$$

Rearranging Equation 8 gives

$$\left(\frac{r_a'}{r_a}\right)^2 = A_{1a}^{-1} = \left(\frac{\lambda_{2a}a_{21}}{a_{21}'}\right)^2 = \left(\frac{\lambda_{3a}a_{31}}{a_{31}'}\right)^2 = \left(\frac{\lambda_{1a}a_{11}}{a_{11}'}\right)^2 \tag{9}$$

Assuming that the orthogonality of *a* and *c* vectors is maintained during deformation, i.e. $(r_a \cdot r_c) = 0$, Equation 9 can be rewritten as

$$\frac{1}{A_{1a}} = \left(\frac{\lambda_{1a}a_{11}}{a_{11}'}\right)^2 = \left(\frac{a_{11}}{\lambda_{1c}a_{11}'}\right)^2 = \left(\frac{\lambda_{2c}\lambda_{3c}a_{11}}{a_{11}'}\right)^2 = \lambda_{2c}^2\lambda_{3c}^2\frac{\sin^2\theta\cos^2\eta}{\sin^2\theta'\cos^2\eta'} \tag{10}$$

Subsequently, one obtains the following expression from Equation 6:

$$A_{3c} = \left(\frac{a_{13}'}{\lambda_{1c}a_{13}}\right)^2 = \left(\frac{a_{13}'\lambda_{2c}\lambda_{3c}}{a_{13}}\right)^2 = \frac{\lambda_{2c}^2\lambda_{3c}^2\cos^2\theta'}{\cos^2\theta} \tag{11}$$

Then

$$\sin^2\theta = 1 - \cos^2\theta = 1 - (\lambda_{2c}^2\lambda_{3c}^2\cos^2\theta'/A_{3c}) = (A_{3c} - \lambda_{2c}^2\lambda_{3c}^2\cos^2\theta')/A_{3c} \tag{12}$$

Rearranging Equation 10 gives

$$\frac{\cos^2\eta}{\cos^2\eta'} = \frac{\sin^2\theta'}{\lambda_{2c}^2\lambda_{3c}^2 A_{1a}\sin^2\theta}$$
$$= \left(\frac{\sin^2\theta'}{\lambda_{2c}^2\lambda_{3c}^2 A_{1a}}\right)\left(\frac{A_{3c}}{A_{23} - \lambda_{2c}^2\lambda_{3c}^2\cos^2\theta'}\right) \quad (13)$$

From the second row of Equation 8 one gets

$$\boldsymbol{r}_a\lambda_{3a}(\sin\varphi\cos\theta\cos\eta + \cos\varphi\sin\eta)$$
$$= \boldsymbol{r}_a'(\sin\varphi'\cos\theta'\cos\eta' + \cos\varphi'\cos\eta') \quad (14)$$

Rearranging Equation 14 gives

$$\sin\varphi'\cos\theta' + \cos\varphi'\tan\eta'$$
$$= \frac{\boldsymbol{r}_a\cos\eta}{\boldsymbol{r}_a'\cos\eta'\lambda_{3c}}(\sin\varphi\cos\theta + \cos\varphi\tan\eta) \quad (15)$$

From Equations 9 and 10,

$$\left(\frac{\boldsymbol{r}_a'}{\boldsymbol{r}_a}\right)^2 = \lambda_{2c}^2\lambda_{3c}^2\frac{\sin^2\theta\cos^2\eta}{\sin^2\theta'\cos^2\eta'}$$
$$\frac{\boldsymbol{r}_a\cos\eta}{\boldsymbol{r}_a'\cos\eta'} = \frac{\sin\theta'}{\lambda_{2c}\lambda_{3c}\sin\theta} \quad (16)$$

Differentiating Equation 15 with respect to η and η' and substituting Equation 16 into Equation 15, one obtains

$$\cos\varphi'\sec^2\eta'\,d\eta' = \frac{\boldsymbol{r}_a\cos\eta}{\boldsymbol{r}_a'\cos\eta'\lambda_{3c}}\cos\varphi\sec^2\eta\,d\eta \quad (17)$$
$$\frac{d\eta}{d\eta'} = \left(\frac{\lambda_{2c}\lambda_{3c}^2\sin\theta}{\sin\theta'}\right)\left(\frac{\cos^2\eta}{\cos^2\eta'}\right)\left(\frac{\cos\varphi'}{\cos\varphi}\right) \quad (18)$$

Substituting Equations 12 and 13 into Equation 18 leads to

$$\frac{d\eta}{d\eta'} = \left(\frac{\lambda_{2c}\lambda_{3c}^2}{\sin\theta'}\right)\left(\frac{(A_{3c} - \lambda_{2c}^2\lambda_{3c}^2\cos^2\theta')^{1/2}}{A_{3c}^{1/2}}\right)$$
$$\times\left(\frac{A_{3c}}{A_{3c} - \lambda_{2c}^2\lambda_{3c}^2\cos^2\theta'}\right)\left(\frac{\sin^2\theta'}{\lambda_{2c}^2\lambda_{3c}^2 A_{1a}}\right)$$
$$\times\left(\frac{\lambda_{2c}(A_{3c} - \lambda_{2c}^2\lambda_{3c}^2\cos^2\theta')^{1/2}}{\sin\theta'}\right) = \frac{A_{3c}^{1/2}}{A_{1a}} \quad (19)$$

Assuming that volume remains unchanged during deformation,

$$\boldsymbol{r}_c'^2\sin\theta'\,d\theta'\,d\varphi'\cdot\boldsymbol{r}_c' = \boldsymbol{r}_c^2\sin\theta\,d\theta\,d\varphi\cdot\boldsymbol{r}_c \quad (20)$$
$$\frac{\boldsymbol{r}_c'^3}{\boldsymbol{r}_c^3} = \frac{1}{A_{3c}^{3/2}} = \frac{\sin\theta\,d\theta\,d\varphi}{\sin\theta'\,d\theta'\,d\varphi'} \quad (21)$$

Finally, the orientation distribution function of crystallites after deformation, $w'(\cos\theta', \varphi', \eta')$, may be expressed as

$$w'(\cos\theta', \varphi', \eta') = w(\cos\theta, \varphi, \eta)\frac{\sin\theta\,d\theta\,d\varphi\,d\eta}{\sin\theta'\,d\theta'\,d\varphi'\,d\eta'}$$
$$= w(\cos\theta, \varphi, \eta)(1/A_{1a}A_{3c}) \quad (22)$$

where $w(\cos\theta, \varphi, \eta)$ represents the orientation distribution function in an undeformed state.

The relationship between the orientation distribution of crystallites, $w(\cos\theta, \varphi, \eta)$, and that of the jth individual crystal planes, $q(\cos\theta_j, \varphi_j)$, may be obtained through the expansion of Jacobi's polynomials up to the expansion coefficient $l = 8$, i.e.

$$w'(\cos\theta', \varphi', \eta')$$
$$= \sum_{l=0}^{8}\sum_{m=-l}^{l}\sum_{n=-l}^{l}[A_{lmn}\cos(m\varphi' + n\eta')$$
$$+ B_{lmn}\sin(m\varphi' + n\eta')]Z_{lmn}(\cos\theta') \quad (23)$$

where the coefficients A_{lmn} and B_{lmn} may be given as

$$\left\{\begin{matrix} A_{lmn} \\ B_{lmn} \end{matrix}\right. = \frac{1}{4\pi^2}\int_{\eta'=0}^{2\pi}\int_{\varphi'=0}^{2\pi}\int_{\theta'=0}^{\pi} w'(\cos\theta', \varphi', \eta')$$
$$\times\left\{\begin{matrix} \cos(m\varphi' + n\eta') \\ \sin(m\varphi' + n\eta') \end{matrix}\right. Z_{lmn}(\cos\theta')\sin\theta'\,d\theta'\,d\varphi'\,d\eta' \quad (24)$$

On the other hand, the orientation distribution function of an individual diffraction plane may be expanded as

$$q^j(\cos_j, \varphi_j) = \sum_{l=0}^{8}\sum_{m=-l}^{l}$$
$$\times[A_{lm}^j\cos m\varphi_j + B_{lm}^j\sin m\varphi_j]$$
$$\times\prod_l^m(\cos\theta_j) \quad (25)$$

Here, the polar angle θ_j and the azimuthal angle φ_j of the $\boldsymbol{r}_j$ vector are defined in Fig. 1. The coefficients A_{lmn} and B_{lmn} in Equation 24 and A_{lm}^j and B_{lm}^j in Equation 25 may be related in terms of the addition theorem of Legendre polynomials

$$\left\{\begin{matrix} A_{lm}^j \\ B_{lm}^j \end{matrix}\right. = 2\pi\left(\frac{2}{2l + 1}\right)^{1/2}\sum_{m=-l}^{l}$$
$$\times\left\{\begin{matrix} A_{lmn}\cos\phi_j - B_{lmn}\sin\phi_j \\ A_{lmn}\sin\phi_j - B_{lmn}\cos\phi_j \end{matrix}\right.\prod_l^n(\cos\Theta_j) \quad (26)$$

$\Pi_l^m(\cos\theta_j)$ and $\Pi_l^n(\cos\Theta_j)$ are the associated Legendre polynomials which may be further related to the Legendre polynomials as follows:

$$Z_{l0n}(\cos\Theta_j) = \prod_l^n(\cos\Theta_j) \quad (27)$$

$$Z_{lm0}(\cos\theta_j) = \prod_l^m(\cos\theta_j) \quad (28)$$

The polar angle Θ_j and the azimuthal angle ϕ_j are already defined in Fig. 1. The angles of (1 1 0), (2 0 0) and (0 2 0) planes of polyethylene are tabulated in Table I based on the orthogonality conditions such as

TABLE I The polar angle Θ_j and azimuthal angle ϕ_j of the individual diffracted planes used in the simulation

Plane	Type 1				Type 2	
	$(\boldsymbol{r}_a\cdot\boldsymbol{r}_c) = 0$		$(\boldsymbol{r}_b\cdot\boldsymbol{r}_c) = 0$		$(\boldsymbol{r}_{110}\cdot\boldsymbol{r}_c) = 0$	
	Θ_j (deg)	ϕ_j (deg)	Θ_j (deg)	ϕ_j (deg)	Θ_j (deg)	ϕ_j (deg)
(1 1 0)	90	56.3	90	−33.7	90	0
(2 0 0)	90	0	90	−90	90	−56.3
(0 2 0)	90	90	90	0	90	33.7

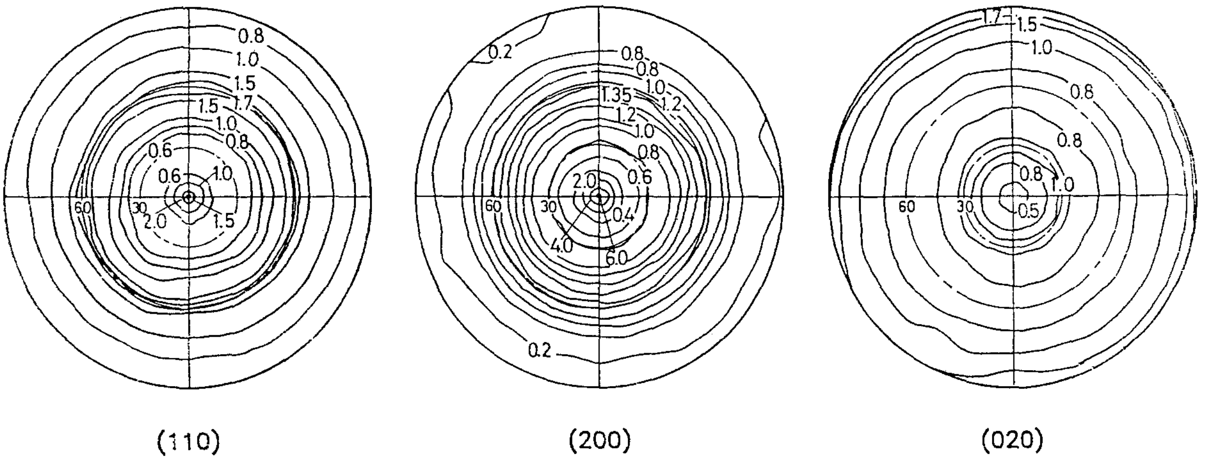

(110) (200) (020)

Figure 2 Pole figures of (1 1 0), (2 0 0) and (0 2 0) crystal planes for the 10 × 10 biaxially stretched film.

$r_a \cdot r_c = 0$ and/or $r_b \cdot r_c = 0$ (Type 1) for crystal orientation and $r_{110} \cdot r_c = 0$ (Type 2) for the {1 1 0} crystal twinning. The physical interpretation of the Type 1 model may be the crystal orientation about the *b* axis, e.g. lamellar detwisting, and/or the crystal rotation about the *a* axis, e.g. chain tilting, respectively. In the case of the Type 2 model, twinning occurs at the {1 1 0} slippage plane.

3. Experimental procedure

UHMWPE used in this study was kindly supplied by Himont Co. The viscosity-average molecular weight M_v of UHMWPE is approximately 6×10^6. The methods of gelation-crystallization and biaxial stretching of the UHMWPE films were thoroughly described in a previous paper [6]. A biaxially stretched film (ratios 10 × 10) was used for WAXD studies. The WAXD pole figures of (1 1 0), (2 0 0) and (0 2 0) crystal planes were acquired on a 12 kW Rigaku X-ray diffractometer with the aid of a pole-figure attachment.

4. Results and discussion

In a previous paper [6] we have qualitatively demonstrated how the pole figures of (1 1 0), (2 0 0) and (0 2 0) planes change with biaxial draw ratio. As mentioned before, the original gelation-crystallized films reveals some preferential *c*-axis orientation in the thickness direction (normal to the film surface). This yields the strong isointensity contours of (2 0 0) and (0 2 0) planes at large polar angles θ_j. The (1 1 0) pole figure shows similar behaviour, as it is the composite of (2 0 0) and (0 2 0) planes. As shown in Fig. 2, the contour lines of the (2 0 0) reflection, upon stretching to a 10 × 10 ratio, become the strongest at the centre with a minor peak at an intermediate polar angle. The maximum peak position of (0 2 0) contour lines remains fairly stationary at large θ_j, and the magnitude also remains unchanged. However, a small shoulder appears at an intermediate polar angle around 30°. As a consequence, there appear two maxima in the pole figure of the (1 1 0) crystal plane, one being located at the centre and the other at an intermediate angle of approximately 60°. This result has been qualitatively interpreted in terms of crystal orientation in which *c*-axis or molecular chains predominantly align in the direction of stretching, such that the *a* axis orients in the thickness direction while the *b* axis partly orients along the direction of stretching.

In order to gain insight into the deformation behaviour, it is essential to analyse the WAXD pole figures quantitatively. It should be borne in mind that the starting gelation-crystallized film has some preferential orientation of *a*- and *b*-axis in the MD*, while the *c* axis aligns in the ND*. The reason for this film-normal orientation of crystal *c*-axis or molecular chain axis may be associated with the large free energy of the surface. Visually, there is some shrinkage in the lateral direction of the gelation-crystallized films. Although the kinematics of the shrinkage may not be the primary cause of the film-normal orientation, it is necessary to know the extent of shrinkage before stretching biaxially. We calculated the orientation distribution functions of the (1 1 0), (0 2 0) and (2 0 0) planes based on the crystal rotation about the crystal *a* axis ($r_b \cdot r_c = 0$), the *b* axis ($r_a \cdot r_c = 0$) or the ⟨1 1 0⟩ plane normal ($r_{110} \cdot r_c = 0$). A shrinkage ratio of 0.85 in the ($r_{110} \cdot r_c = 0$) mode gives the best fit between the model calculation and the experimental results

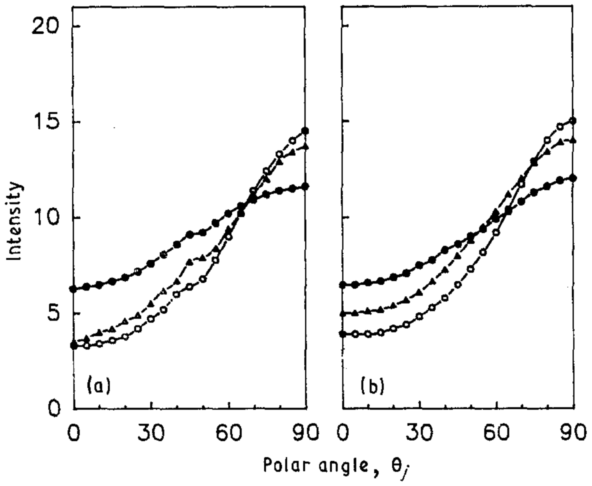

Figure 3 A comparison of (a) experimental and (b) calculated intensity profiles of the original gelation-crystallized UHMWPE film before stretching. (○) (1 1 0), (●) (2 0 0), (△) (0 2 0).

---

* MD = machine direction; ND = normal direction

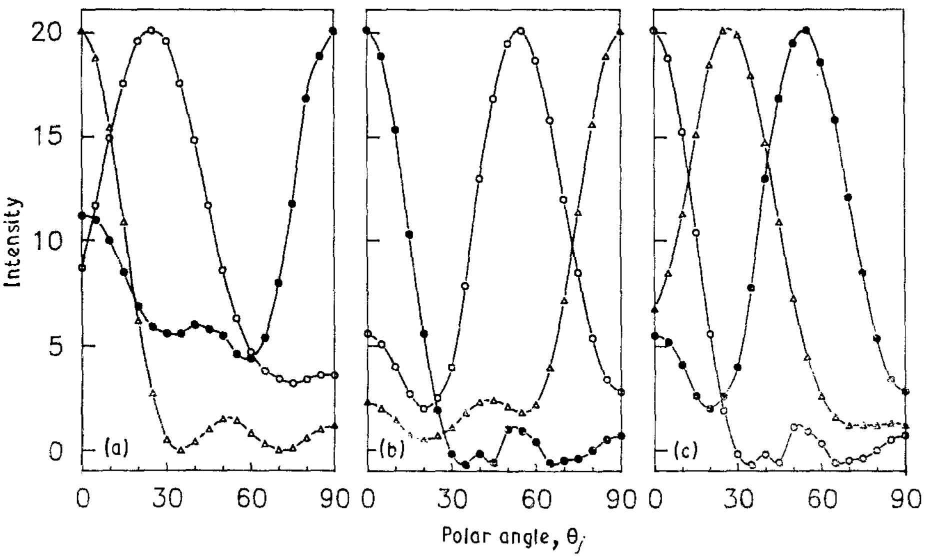

Figure 4 Simulated intensity profiles for crystal orientations based on the models (a) $r_b \cdot r_c = 0$, (b) $r_a \cdot r_c = 0$ and crystal twinning (c) $r_{110} \cdot r_c = 0$. (○) (1 1 0), (●) (2 0 0), (△) (0 2 0).

(Fig. 3). The value $\lambda = 0.85$ will be used as the starting draw ratio for biaxial stretching.

Fig. 4 illustrates the comparison of the intensity profiles of the orientation distribution functions of the reciprocal lattice vectors ($2\pi q_j$) of (1 1 0), (2 0 0) and (0 2 0) planes based on the model calculations for two types of crystal orientations (i.e. the crystal rotation around the *a* axis and around the *b* axis) and the crystal twinning at the {1 1 0} slippage plane. As a first step, a biaxial draw ratio of 1.8 × 1.8 was arbitrarily chosen in the calculation in order to see the trend of the intensity variation with polar angle. The first model of crystal rotation around the *a* axis ($r_b \cdot r_c = 0$) shows the opposite trend as compared with the experimental intensity profiles of (2 0 0) and (0 2 0) planes (Fig. 3); thus it may be ruled out. The second model of crystal rotation around the *b* axis ($r_a \cdot r_c = 0$) exhibits a right trend of the orientation behaviour of reciprocal lattice vectors of the (2 0 0) plane. In the case of the (0 2 0) plane, the model predicts a strong intensity at the polar angle of 90°, but it fails to account for the intermediate peak at about 30°. As for the (1 1 0) plane, the model predicts very well for the peak at a polar angle of 60°; however, the peak at 0° is too weak relative to the experimental result. The combined orientation models evidently cannot adequately account for the observed intensity profiles. This implies the need for further considering additional mechanisms, such as crystal transformation and/or twinning.

As demonstrated in a previous paper [6], the crystal transformation from orthorhombic to monoclinic phase was not detected in these biaxially stretched gelation-crystallized UHMWPE films, although such a phenomenon was often seen in compression moulded [9] or cold-rolled [1] polyethylene films. Hence, the mechanism of crystal transformation may be ruled out for the biaxial stretching. In the deformation of polyethylene crystals, {1 1 0} and {3 1 0} twinning has been known to occur. However, only {1 1 0} twinning was observed during the deformation of polyethylene single crystals without any evidence of {3 1 0} twinning [10, 11]. In the present case, no evidence was again found for the {3 1 0} twins. We then calculated the {1 1 0} crystal twinning and the results are shown in Fig. 4 in comparison with those of the orientation model. The crystal twinning model fails to explain the overall behaviour of intensity profiles. However, it predicts the strong intensity of reciprocal lattice vectors of the (1 1 0) plane at $\theta_j = 0°$ and that of (0 2 0) at $\theta_j = 30°$. These two peaks are exactly what the model of crystal rotation around the *b* axis fails to predict; which in turn suggests that both the crystal

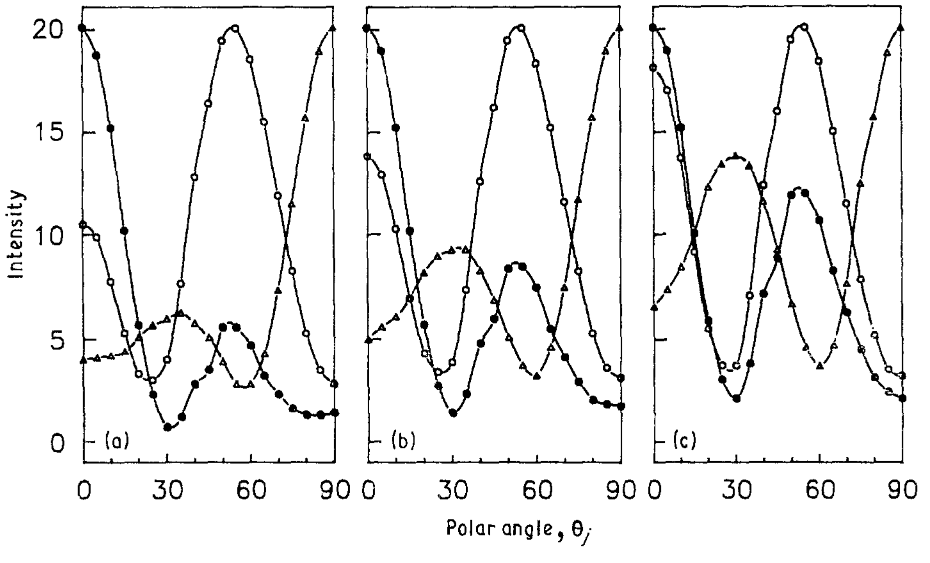

Figure 5 Intensity profiles calculated by taking into account the relative contributions of crystal twinning and orientation at the 1.8 × 1.8 draw ratio: (a) 20:80, (b) 30:70 and (c) 40:60. (○) (1 1 0), (●) (2 0 0), (△) (0 2 0).

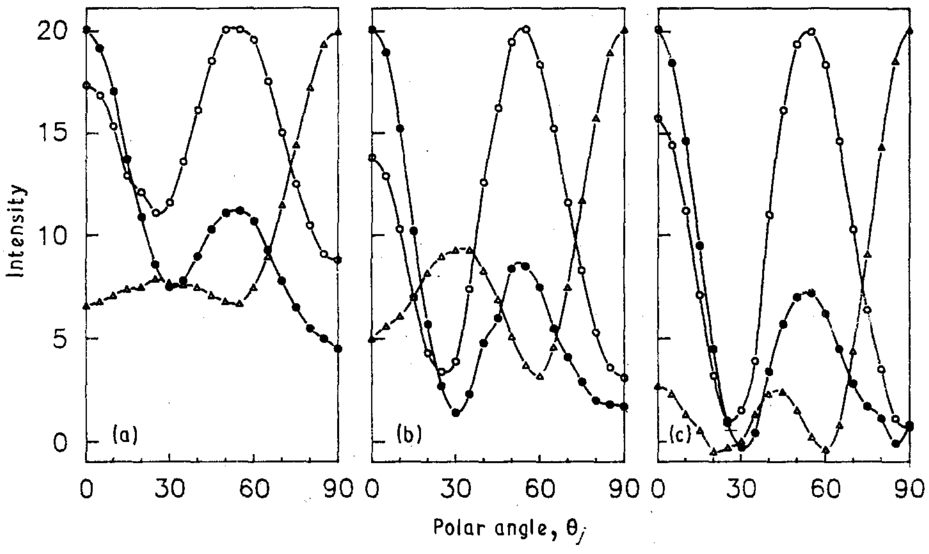

Figure 6 Intensity profiles of the 30:70 twinning/orientation for draw ratios (a) 1.5 × 1.5, (b) 1.8 × 1.8 and (c) 2.0 × 2.0. (○) (1 1 0), (●) (2 0 0), (△) (0 2 0).

orientation ($\boldsymbol{r}_a \cdot \boldsymbol{r}_c = 0$) and the {1 1 0} crystal twinning might occur concurrently during biaxial drawing of the gelation-crystallized UHMWPE films.

The relative contribution of the crystal orientation and the crystal twinning at the {1 1 0} plane for a given biaxial draw ratio of 1.8 × 1.8 has been evaluated based on the affine assumption. As can be seen in Fig. 5, the model simulation of 70% crystal orientation and 30% crystal twinning gives the best fit with the experimental intensity profiles for the 10 × 10 specimen shown in Fig. 3. Next, we examine the effect of stretching ratio by fixing the contributions at 70% crystal orientation and 30% twinning. As shown in Fig. 6, for a low draw ratio of 1.5 × 1.5 the calculated (0 2 0) peak at 30° turns out to be small, whereas at a high draw ratio of 2.0 × 2.0 the (0 2 0) intensity oscillates about zero. The calculated intensity profiles for the biaxial draw ratio of 1.8 × 1.8 yields the best fit with the experimental data (Fig. 7). Strictly speaking, the (2 0 0) intensity is slightly higher than the experimental one, which may be due to the fact that the crystal rotation around the *a* axis was totally ignored in the model calculation. It is reasonable to conclude that the affine model with the contribution of 70% crystal orientation and 30% twinning is valid up to the draw ratio of 1.8 × 1.8, and then the calculated intensity deviates from ideality with increasing biaxial draw ratio. The validity of the affine assumption has recently been tested by neutron scattering experiments of uniaxial deformation [12–14]. The orientation of linear polyethylene chains appears to hold only up to the draw ratio of approximately 5 [13, 14].

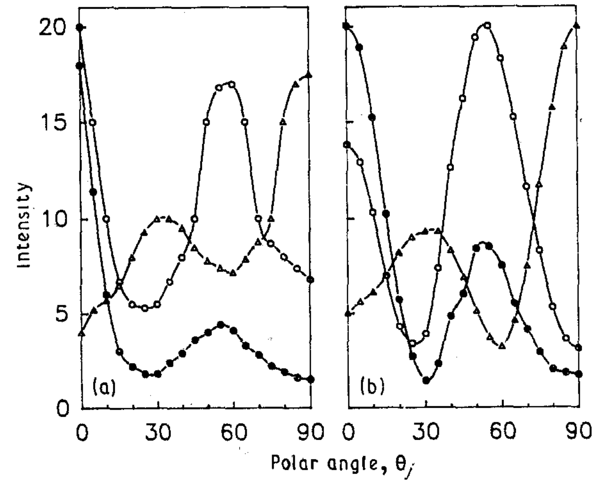

Figure 7 A comparison of (a) observed and (b) calculated intensity profiles, based on the affine assumption with a 30:70 twinning/orientation and at a 1.8 × 1.8 draw ratio. (○) (1 1 0), (●) (2 0 0), (△) (0 2 0).

5. Conclusions

In the quantitative examination of the WAXD pole figures, crystal rotation around the *b* axis appears to be the dominant mechanism. However, the crystal orientation alone fails to account for the intensity profiles of the orientation distribution function of the reciprocal lattice vectors of (1 1 0) and (0 2 0) planes. {1 1 0} twinning has to be taken into account to explain the biaxial deformation behaviour of the gelation-crystallized UHMWPE films. The crystal transformation from orthorhombic to monoclinic phase which has been known to occur in cold-rolled polyethylenes was not observed during the simultaneous biaxial stretching.

Acknowledgement

The support of this work by the National Science Foundation (Grant No. MSM 87-13531) is gratefully acknowledged.

References

1. F. C. FRANK, A. KELLER and A. O'CONNOR, *Phil. Mag.* **3** (1958) 64.
2. P. H. GEIL, H. KIHO and A. PETERLIN, *J. Polym. Sci. B* **2** (1964) 71.
3. H. KIHO, A. PETERLIN and P. H. GEIL, *J. Appl. Phys.* **35** (1964) 1599.
4. *Idem, J. Polym. Sci. B* **3** (1965) 263.
5. K. HAAS and P. H. GEIL, *J. Polym. Sci. A-2* **4** (1966) 298.
6. T. KYU, K. FUJITA and M. H. CHO, *Polym. Eng. Sci.* **29** (1989) 383.

7. S. HIBI, M. MAEDA, A. YOKOYAMA, K. FUJITA and N. KURATA, *Kobunshi Ronbunshu* **42** (1985) 63.
8. K. SUZUKI, S. HIBI, T. TORII, M. KOBAYASHI, E. NAKANISHI and M. MAEDA, *ibid.* **44** (1987) 491.
9. T. SETO, T. HARA and K. TANAKA, *J. Appl. Phys.* **7** (1968) 31.
10. P. ALLAN, E. B. CRELLIN and M. BEVIS, *Phil. Mag.* **27** (1973) 127.
11. R. J. YOUNG and P. B. BOWDEN, *ibid.* **29** (1974) 1061.
12. R. S. STEIN, C. T. MURRAY, H. YANG, V. SONI and R. J. LO, *Physica* **137B** (1986) 194.
13. R. J. LO, PhD dissertation, University of Massachusetts (1986).
14. D. M. SADLER and P. J. BARHAM, *Polymer* **31** (1990) 43.

Received 7 February
and accepted 19 February 1990